An Exact Analysis of Low Peclet Number Thermal Entry Region Heat Transfer in Transversely Nonuniform Velocity Fields

CHIA-JUNG HSU

Brookhaven National Laboratory, Upton, New York

A theoretical method is described for obtaining the exact solution to the problem of thermal entry region heat transfer which takes into account both transverse nonuniformity in the velocity field and axial conduction. To allow for the effect of upstream conduction, the fluid temperature was taken to be uniform at $x = -\infty$, and the first 20 eigenvalues and the corresponding eigenfunctions were determined separately for the heated and adiabatic regions. Both the temperatures and temperature gradients were then matched at $x = 0$ by constructing a pair of orthonormal functions from the nonorthogonal eigenfunctions.

Nusselt numbers calculated for pipe flow subject to the boundary condition of uniform wall heat flux show virtually perfect agreement with those reported recently by Hennecke, who solved the governing partial differential equation numerically. To illustrate its general applicability, the present method was further employed to analyze the corresponding problem in parallel-plate channel flow, for which no solution has hitherto been reported.

Heretofore, no method has been available for obtaining a theoretical solution to the problem of thermal entry region heat transfer in channel flow, taking into account both transverse nonuniformity of fluid velocity and axial conduction in the flowing fluid. This problem is mathematically quite intricate, because, with such a velocity field, the elliptic energy equation containing the axial conduction term gives rise to a Whittaker-type differential equation (*8*) for which the determination of eigenconstants is difficult. Moreover, because the eigenfunctions lack the property of orthogonality, the eigenfunction expansion technique customarily employed for the differential equations of the Sturm-Liouville system no longer applies. To remedy these difficulties, the present author proposed (*4*) a method of solving the axial-conduction problem by directly computing the eigenconstants for the Whittaker differential equation. In that analysis, fluid temperature was assumed to be uniform at the point ($x = 0$) where a step change in wall heat flux is imposed. Such a boundary condition, although physically unrealistic, has been frequently employed in slug flow or numerical analysis of the corresponding problem (*5, 9, 10*). In reality, however, because of the heat conducted upstream, transverse variation in fluid temperature exists in the region $x \leq 0$. This was first shown by Petukhov and Tsvetkov (*7*), who considered the flow channel to extend from $x = -\infty$ to $x = \infty$, and obtained approximate temperature solutions by solving the governing energy equation numerically. Recently, Hennecke (*3*) also solved the governing partial differential equation numerically by employing the finite-difference method, and obtained temperature solutions for the boundary conditions of both uniform wall temperature and uniform wall heat flux. All of these authors found that the temperature profile at $x = 0$ is greatly affected by axial conduction, and consequently the thermal entry region Nusselt numbers behave quite differently from those obtained by assuming a flat temperature profile at $x = 0$.

The purpose of this study was to develop a mathematical method for obtaining an exact solution to the present heat transfer problem. By the method described in this paper, the calculated Nusselt numbers were found to be in excellent agreement with those obtained numerically by Hennecke (*3*). To show the general applicability of the method, it was further used to analyze the analogous problem in parallel-plate channel flow, for which no results have been reported in the literature.

It should be mentioned that Agrawal (*1*) was the only other author who has attempted to seek an analytical solution to a similar problem. He sought the eigenfunctions in the form of infinite Fourier sine series and obtained the solution corresponding to $N_{Pe} = 1$ for a parallel-plate channel subject to a step change in wall temperature at $x = 0$. His approach, however, is extremely complex. Furthermore, his computational results show poor matching of the temperature solutions at $x = 0$. The accuracy of the Nusselt number curve, which was reported only for $N_{Pe} = 1$, is therefore subject to considerable doubt.

In the present study, the first 20 eigenconstants were determined for the adiabatic ($-\infty < x \leq 0$) and heated ($0 \leq x < \infty$) regions separately. Both the temperatures and longitudinal temperature gradients were then matched at $x = 0$. To accomplish the matching processes, two new sets of orthonormal functions were constructed from the nonorthogonal eigenfunctions, utilizing the Gram-Schmidt orthonormalization procedure (*6*). By employing the orthonormal functions, the series expansion coefficients were determined by solving the relevant matrix equations so that the required matching conditions at $x = 0$ were both satisfied. In the following treatment, the discussion will be based on laminar pipe flow, which is subject to a step change in wall heat flux at $x = 0$. Modification of the analysis for application to parallel-plate channel flow is simple and only a brief treatment here is necessary.

THEORETICAL ANALYSIS

It is now evident that the problem posed here is to seek the temperature solutions to the following system of energy equations:

$$2\rho \bar{u} C_p [1 - (r/r_o)^2] \frac{\partial T_i}{\partial x} = k \left[\frac{\partial^2 T_i}{\partial r^2} + \frac{1}{r} \frac{\partial T_i}{\partial r} + \frac{\partial^2 T_i}{\partial x^2} \right] \quad (i = 1, 2) \quad (1)$$

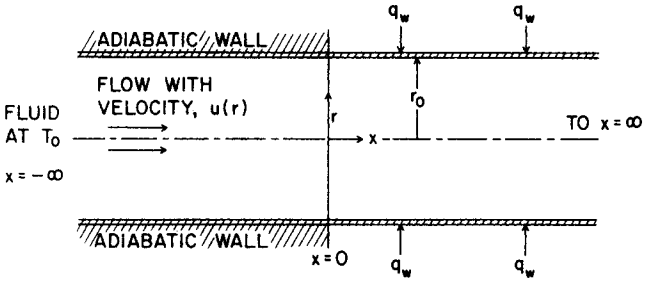

Fig. 1. Coordinate system for the flow channel (pipe).

where $i = 1$ and 2 refers, respectively, to the region $-\infty < x \leq 0$ and $0 \leq x < \infty$, as sketched in Figure 1. The appropriate boundary conditions to be satisfied are

For $-\infty < x \leq 0$:

$$\frac{\partial T_1}{\partial r}(x,0) = \frac{\partial T_1}{\partial r}(x,r_o) = 0; \quad T_1(-\infty,r) = T_o \tag{2}$$

For $0 \leq x < \infty$:

$$\frac{\partial T_2}{\partial r}(x,0) = 0; \quad k\frac{\partial T_2}{\partial r}(x,r_o) = q_w \tag{3a}$$

$$T_2 = T_{fd} \quad \text{as} \quad x \longrightarrow \infty \tag{3b}$$

At $x = 0$:

$$T_1(0,r) = T_2(0,r); \quad \frac{\partial T_1}{\partial x}(0,r) = \frac{\partial T_2}{\partial x}(0,r) \tag{4}$$

In Equation (3b), T_{fd} refers to the fully developed temperature profile which includes the effect of axial conduction. Its derivation will be given below. The boundary condition, Equation (3b), implies that for sufficiently large x, T_2 should reduce to T_{fd}. It is essentially equivalent to the boundary condition: $\partial T_2/\partial x = 2q_w/\rho C_p \bar{u} r_o$ as $x \longrightarrow \infty$. By letting $\theta_i = (T_i - T_o)/(q_w r_o/k)$, $(i = 1,2)$, $\eta = x/r_o N_{Pe}$, $\xi = r/r_o$, Equations (1) through (4) can be transformed to

$$(1-\xi^2)\frac{\partial \theta_i}{\partial \eta} = \left[\frac{\partial^2 \theta_i}{\partial \xi^2} + \frac{1}{\xi}\frac{\partial \theta_i}{\partial \xi} + \frac{1}{N_{Pe}^2}\frac{\partial^2 \theta_i}{\partial \eta^2}\right] \quad (i = 1,2) \tag{5}$$

For $-\infty < \eta \leq 0$:

$$\frac{\partial \theta_1}{\partial \xi}(\eta,1) = \frac{\partial \theta_1}{\partial \xi}(\eta,0) = 0 \tag{6a}$$

$$\theta_1(-\infty,\xi) = 0 \tag{6b}$$

For $0 \leq \eta < \infty$:

$$\frac{\partial \theta_2}{\partial \xi}(\eta,0) = 0 \tag{7a}$$

$$\frac{\partial \theta_2}{\partial \xi}(\eta,1) = 1 \tag{7b}$$

$$\theta_2 = \theta_{fd} \quad \text{as} \quad \eta \longrightarrow \infty \tag{7c}$$

At $\eta = 0$:

$$\theta_1(0,\xi) = \theta_2(0,\xi) \tag{8a}$$

$$\frac{\partial \theta_1}{\partial \eta}(0,\xi) = \frac{\partial \theta_2}{\partial \eta}(0,\xi) \tag{8b}$$

An expression for θ_{fd} can be obtained by noting that it can be expressed in the form (see, for example, reference 2)

$$\theta_{fd} = 4\eta + \xi^2 - \frac{\xi^4}{4} + C_1 \tag{9}$$

where C_1 is an integration constant. To determine C_1, a heat balance is taken over the region extending from $x = -\infty$ to an arbitrary axial position in the fully developed region. Thus, let $\bar{\theta}_{fd}$ denote the dimensionless average fluid temperature in the fully developed region. Then one obtains

$$\bar{\theta}_{fd} = 4\eta + \frac{4}{N_{Pe}^2}\int_0^1 \xi(\partial\theta_{fd}/\partial\eta)\,d\xi = 4\eta + \frac{8}{N_{Pe}^2} \tag{10}$$

Since the average fluid temperature $\bar{\theta}_\eta$ at any axial position η is given by the general expression

$$\bar{\theta}_\eta = 4\int_0^1 \xi(1-\xi^2)\theta_\eta\,d\xi \tag{11}$$

substitution of Equation (9) into Equation (11), followed by integration and comparison with Equation (10), give $C_1 = (8/N_{Pe}^2) - (7/24)$. The fully developed temperature solution including the effect of axial conduction is thus found to be

$$\theta_{fd} = 4\eta + \xi^2 - \frac{\xi^4}{4} - \frac{7}{24} + \frac{8}{N_{Pe}^2} \tag{12}$$

which differs from that for the case where axial conduction is neglected by containing the additional term, $8/N_{Pe}^2$. The boundary condition, Equation (7c), is now completely specified. To solve for θ_2, it is convenient to further let $\theta_2 = \Theta_2 + \theta_{fd}$, where Θ_2 now has to satisfy the equation

$$(1-\xi^2)\frac{\partial \Theta_2}{\partial \eta} = \left[\frac{\partial^2 \Theta_2}{\partial \xi^2} + \frac{1}{\xi}\frac{\partial \Theta_2}{\partial \xi} + \frac{1}{N_{Pe}^2}\frac{\partial^2 \Theta_2}{\partial \eta^2}\right] \tag{13}$$

with

$$\frac{\partial \Theta_2}{\partial \xi}(\eta,0) = \frac{\partial \Theta_2}{\partial \xi}(\eta,1) = 0 \tag{14a}$$

$$\Theta_2(\infty,\xi) = 0 \tag{14b}$$

The temperature solutions θ_1 and Θ_2 are now sought in the form

$$\theta_1 = \sum_{n=1}^{\infty} B_n Y_n(\xi)\exp[\alpha_n^2\eta] \tag{15a}$$

$$\Theta_2 = \sum_{n=1}^{\infty} C_n R_n(\xi)\exp[-\beta_n^2\eta] \tag{15b}$$

which satisfies, respectively Equation (6b) and Equation (14b). On substituting Equation (15a) into Equations (5) and (6), it can be proved that Equation (15a) indeed satisfies the latter equations, provided that α_n and $Y_n(\xi)$ are the eigenvalues and eigenfunctions, respectively, of the following characteristic equation:

$$\frac{d^2Y_n}{d\xi^2} + \frac{1}{\xi}\frac{dY_n}{d\xi} + \alpha_n^2\left[\frac{\alpha_n^2}{N_{Pe}^2} - (1-\xi^2)\right]Y_n = 0 \tag{16}$$

satisfying the boundary conditions:

$$\frac{dY_n}{d\xi} = 0 \quad \text{at } \xi = 0 \text{ and } \xi = 1. \tag{17}$$

Similarly, substituting Equation (15b) into Equations (13) and (14) yields the following characteristic equation:

$$\frac{d^2R_n}{d\xi^2} + \frac{1}{\xi}\frac{dR_n}{d\xi} + \beta_n^2\left[\frac{\beta_n^2}{N_{Pe}^2} + (1-\xi^2)\right]R_n = 0 \tag{18}$$

with the boundary conditions

$$\frac{dR_n}{d\xi} = 0 \quad \text{at } \xi = 0 \text{ and } \xi = 1 \tag{19}$$

It is worth noting that, as $N_{Pe} \longrightarrow \infty$, Equation (18) reduces to the characteristic equation for the Graetz-type problem which neglects axial conduction. The eigenvalues α_n and β_n and the corresponding eigenfunctions Y_n and R_n of the above two characteristic equations were determined in this study by solving these equations using the Runge-Kutta method. The computed first 20 eigenvalues α_n and β_n are tabulated in Table 1* for $N_{Pe} = 1$ and 5. The first 10 $R_n(\xi)$ and the first six $Y_n(\xi)$ are shown graphically in Figures 2 through 4 for $N_{Pe} = 1$. The β_n values (but not α_n) for other Peclet numbers can be found in the previous paper (*4*), where it was pointed out that for $N_{Pe} > 100$, both β_n and R_n vary only slightly with further increase in Peclet number; they eventually approach asymptotically toward those for $N_{Pe} = \infty$ (no axial conduction). By incorporating Equation (12) with Equation (15*b*) the temperature solution θ_2 for the region $0 \leq x < \infty$ can now be summarized in the form

$$\theta_2 = 4\eta + \xi^2 - \frac{\xi^4}{4} - \frac{7}{24} + \frac{8}{N_{Pe}^2} + \sum_{n=1}^{\infty} C_n R_n(\xi) \exp\left[-\beta_n^2 \eta\right] \quad (20)$$

After determining the eigenconstants, it still remains to find the series expansion coefficients B_n's and C_n's in Equations (15) so that the boundary conditions at $\eta = 0$, that is, Equations (8*a*) and (8*b*), are both satisfied. From Equations (15*a*) and (20), these two conditions are seen to be equivalent to

$$\sum_{n=1}^{\infty} C_n R_n(\xi) - \sum_{n=1}^{\infty} B_n Y_n(\xi) = -\left[\xi^2 - \frac{\xi^4}{4} - \frac{7}{24} + \frac{8}{N_{Pe}^2}\right] \quad (21a)$$

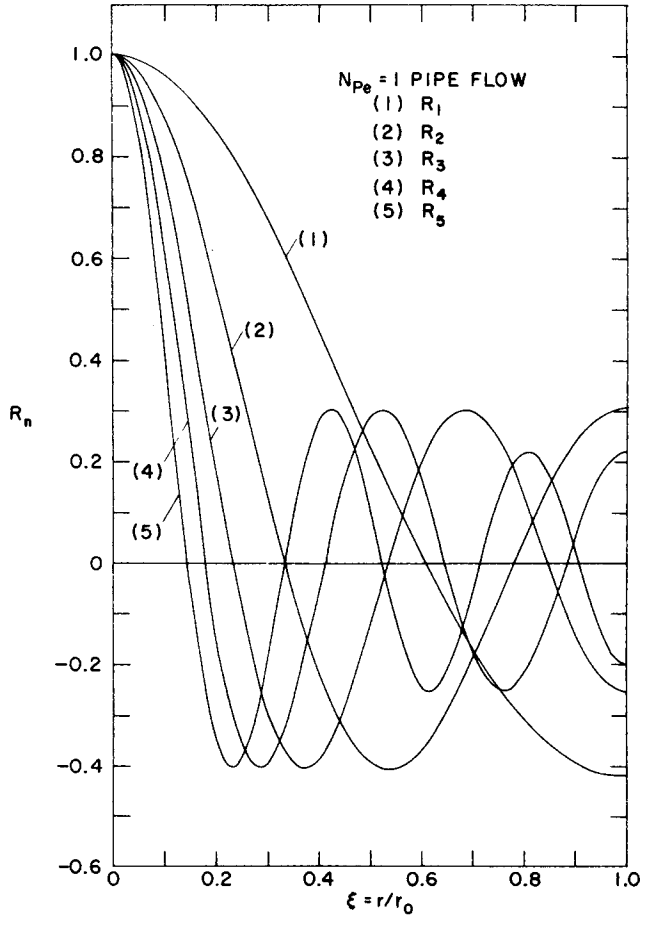

Fig. 2. Eigenfunctions $R_1 \sim R_5$ for pipe flow ($N_{Pe} = 1$).

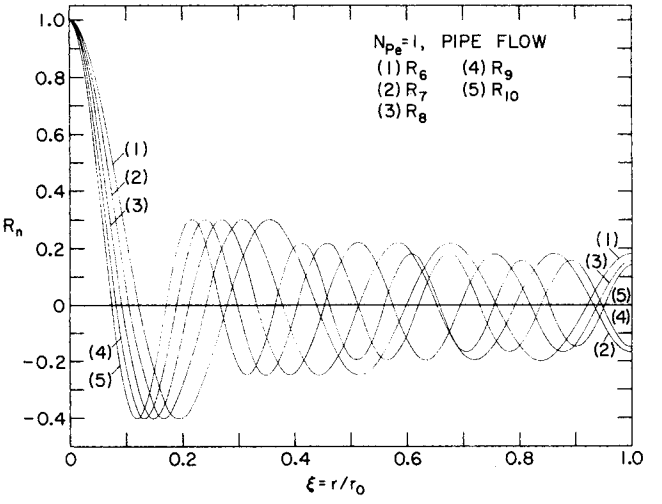

Fig. 3. Eigenfunctions $R_6 \sim R_{10}$ for pipe flow ($N_{Pe} = 1$).

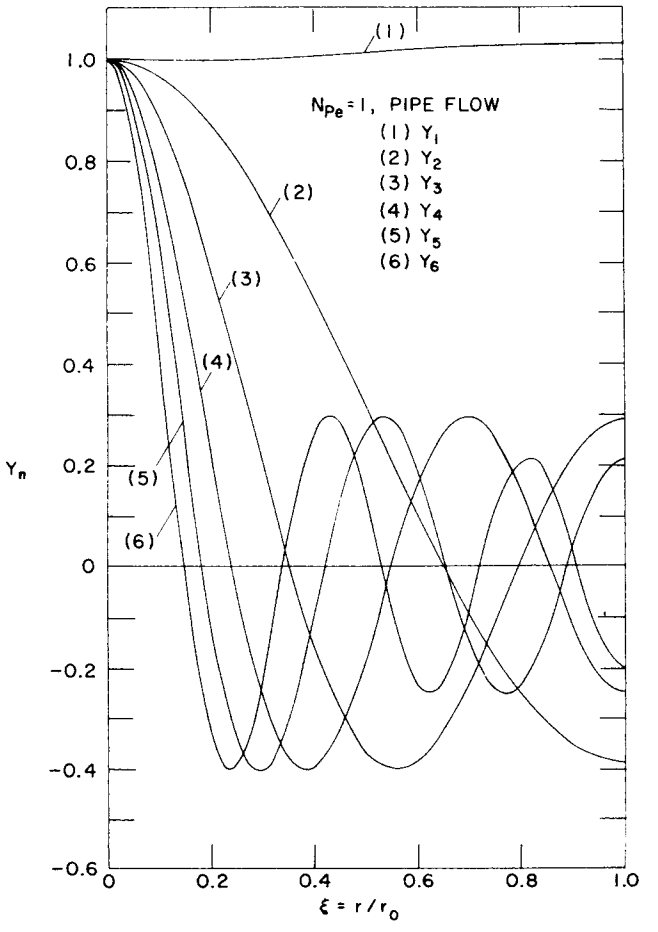

Fig. 4. Eigenfunctions $Y_1 \sim Y_6$ for pipe flow ($N_{Pe} = 1$).

*Tables 1 through 6 have been deposited as document No. 01384 with the ASIS National Auxiliary Publications Service, c/o CCM Information Sciences, Inc., 909 Third Ave., New York 10022 and may be obtained for $2.00 for microfiche or $5.00 for photocopies.

$$\sum_{n=1}^{\infty} C_n \beta_n^2 R_n(\xi) + \sum_{n=1}^{\infty} B_n \alpha_n^2 Y_n(\xi) = 4 \qquad (21b)$$

Neither R_n nor Y_n are orthogonal functions, as can be theorized from the form of Equations (16) and (18). This constitutes the main drawback to the present problem, since the widely used Fourier series expansion technique becomes inapplicable for determining the series expansion coefficients. To overcome this difficulty, two artificial sets of orthonormal functions are constructed using $R_n(\xi)$ and $Y_n(\xi)$. It is known (see, for example, reference 6) from the theory of functions of a real variable that, given in the Hilbert space a finite or denumerable linear independent system of functions, $R_1(\xi)$, $R_2(\xi)$ $\cdots$ on a closed interval $[a, b]$, it is possible to construct an orthonormal system $\psi_1(\xi)$, $\psi_2(\xi)$, $\cdots$ such that each $\psi_n(\xi)$ is a linear combination of the first n functions of the system $R_n(\xi)$. Let $\psi_j(\xi)$ and $\phi_j(\xi)$ be the two new sets of orthonormal functions to be constructed; then they can be expressed in terms of R_n and Y_n in the following form:

$$\psi_j = \sum_{n=1}^{j} a_n^j R_n(\xi), \quad j = 1, 2, \cdots \qquad (22a)$$

$$\phi_j = \sum_{n=1}^{j} b_n^j Y_n(\xi), \quad j = 1, 2, \cdots \qquad (22b)$$

for which

$$\int_0^1 \psi_i \psi_j d\xi = \begin{cases} 0 \text{ if } i \neq j \\ 1 \text{ if } i = j \end{cases}; \quad \int_0^1 \phi_i \phi_j d\xi = \begin{cases} 0 \text{ if } i \neq j \\ 1 \text{ if } i = j \end{cases} \qquad (23)$$

The orthonormalization can be carried out step by step; for example

$$\psi_1 = \frac{R_1(\xi)}{\sqrt{\Delta_1}}, \quad \psi_2 = \frac{\begin{vmatrix} \int_0^1 R_1^2 d\xi & R_1 \\ \int_0^1 R_2 R_1 d\xi & R_2 \end{vmatrix}}{\sqrt{\Delta_1 \cdot \Delta_2}}, \text{ etc.}$$

and, in general

$$\psi_n = \frac{\begin{vmatrix} \int_0^1 R_1^2 d\xi & \int_0^1 R_1 R_2 d\xi & \cdots & \cdots & \int_0^1 R_1 R_{n-1} d\xi & R_1(\xi) \\ \int_0^1 R_2 R_1 d\xi & \int_0^1 R_2^2 d\xi & \cdots & \cdots & \int_0^1 R_2 R_{n-1} d\xi & R_2(\xi) \\ \cdots & \cdots & \cdots & \cdots & \cdots & \cdots \\ \cdots & \cdots & \cdots & \cdots & \cdots & \cdots \\ \int_0^1 R_n R_1 d\xi & \int_0^1 R_n R_2 d\xi & \cdots & \cdots & \int_0^1 R_n R_{n-1} d\xi & R_n(\xi) \end{vmatrix}}{\sqrt{\Delta_n \Delta_{n-1}}} \qquad (24)$$

where Δ_n is the Gram determinant defined by

$$\Delta_n = \begin{vmatrix} \int_0^1 R_1^2 d\xi & \int_0^1 R_1 R_2 d\xi & \cdots & \int_0^1 R_1 R_{n-1} d\xi & \int_0^1 R_1 R_n d\xi \\ \int_0^1 R_2 R_1 d\xi & \int_0^1 R_2^2 d\xi & \cdots & \int_0^1 R_2 R_{n-1} d\xi & \int_0^1 R_2 R_n d\xi \\ \cdots & \cdots & \cdots & \cdots & \cdots \\ \cdots & \cdots & \cdots & \cdots & \cdots \\ \cdots & \cdots & \cdots & \cdots & \cdots \\ \int_0^1 R_n R_1 d\xi & \int_0^1 R_n R_2 d\xi & \cdots & \int_0^1 R_n R_{n-1} d\xi & \int_0^1 R_n^2 d\xi \end{vmatrix} \qquad (25)$$

By employing the computed values of $R_n(\xi)$ and $Y_n(\xi)$, $\psi_n(\xi)$ and $\phi_n(\xi)$ were constructed in this study for $n = 1 \sim 20$. Some of the numerical constants a_n^j and b_n^j are tabulated in Table 2* for $N_{Pe} = 1$ and 5. To make Equations (22) appropriate for determining the series expansion coefficients, it is further necessary to express $R_n(\xi)$ and $Y_n(\xi)$ in terms of the new system of functions $\psi_j(\xi)$ and $\phi_j(\xi)$, that is

$$R_j = \sum_{n=1}^{j} p_n^j \psi_n(\xi) \qquad (26a)$$

$$Y_j = \sum_{n=1}^{j} q_n^j \phi_n(\xi) \qquad (26b)$$

The coefficients p_n^j and q_n^j were computed by writing Equation (22) in the form of a matrix equation, and then inverting the matrices containing a_n^j and b_n^j. Some of the numerical constants p_n^j and q_n^j are tabulated in Table 3* for $N_{Pe} = 1$ and 5. Substituting Equations (26) into Equations (21), one obtains

$$\sum_{n=1}^{\infty} \sum_{j=n}^{\infty} C_j p_n^j \psi_n(\xi) - \sum_{n=1}^{\infty} \sum_{j=n}^{\infty} B_j q_n^j \phi_n(\xi) = f_1(\xi) \qquad (27a)$$

$$\sum_{n=1}^{\infty} \sum_{j=n}^{\infty} C_j \beta_j^2 p_n^j \psi_n(\xi) + \sum_{n=1}^{\infty} \sum_{j=n}^{\infty} B_j \alpha_j^2 q_n^j \phi_n(\xi) = 4 \qquad (27b)$$

where $f_1(\xi) = -\left[\xi^2 - \frac{\xi^4}{4} - \frac{7}{24} + (8/N_{Pe}^2)\right]$. The above two equations now make it possible to determine the series expansion coefficients C_n's and B_n's, inasmuch as ψ_n and ϕ_n are orthonormal functions. Thus, by multiplying Equation (27a) by ψ_m and Equation (27b) by ϕ_m, and then integrating from 0 to 1, one obtains, as a consequence of the orthonormal properties given by Equation (23), the following

*See footnote on p. 734.

set of equations:

$$\sum_{j=m}^{\infty} C_j p_m^j - \sum_{n=1}^{\infty} \sum_{j=n}^{\infty} B_j q_n^j \int_0^1 \phi_n \psi_m d\xi = \int_0^1 f_1(\xi) \psi_m d\xi \quad (28a)$$

$$\sum_{j=m}^{\infty} B_j \alpha_j^2 q_m^j + \sum_{n=1}^{\infty} \sum_{j=n}^{\infty} C_j \beta_j^2 p_n^j \int_0^1 \psi_n \phi_m d\xi = 4 \int_0^1 \phi_m d\xi, \quad (m = 1, 2, \cdots) \quad (28b)$$

In this study the infinite series appearing in the above two equations were truncated at $m = 20$, since larger values of m were found to yield negligible improvement in the accuracy of the series expansion coefficients. With $m = 20$, Equations (28) give rise to 40 linear equations relating the forty unknowns $C_1 \sim C_{20}$ and $B_1 \sim B_{20}$. The system of simultaneous linear equations was solved by using the Gauss elimination method. Thus let

Then $\vec{F}$ can be obtained from the following equation:

$$\vec{F} = \vec{E}^{-1} \vec{G} \quad (30)$$

For the actual computation using the computer, the matrices were normalized rowwise by dividing by the largest element of $E(i, j)$ in that row. The $\vec{E}$ matrix was then reduced to triangular form by $(n - 1)$ transformations using a pivotal condensation process. For larger Peclet numbers (say, $20 < N_{Pe} < 100$), Equation (30) was found to give satisfactory results. For smaller Peclet numbers, however, it was found necessary to further improve the accuracy by an iteration process using Equation (28a) and Equation (28b). In any case, the iterative calculation was continued until virtually complete satisfaction with both Equation (21a) and Equation (21b) was obtained. The C_n and B_n coefficients thus obtained are tabulated in Table 1 for $N_{Pe} = 1$ and 5.

Having determined the series expansion coefficients, the two temperature solutions θ_1 and θ_2 given, respectively, by Equation (15a) and Equation (20), are now complete. The equation for cup-mixing average fluid temperature in the heated region, for instance, can be derived by substituting

$$\vec{F} = \begin{pmatrix} C_1 \\ \cdot \\ \cdot \\ \cdot \\ C_m \\ B_1 \\ B_2 \\ \cdot \\ \cdot \\ \cdot \\ B_m \end{pmatrix} \quad (29a)$$

$$\vec{G} = \begin{pmatrix} \int_0^1 f_1 \psi_1 d\xi \\ \cdot \\ \cdot \\ \cdot \\ \int_0^1 f_1 \psi_m d\xi \\ 4 \int_0^1 \phi_1 d\xi \\ \cdot \\ \cdot \\ \cdot \\ 4 \int_0^1 \phi_m d\xi \end{pmatrix} \quad (29b)$$

and

$$\vec{E} = \begin{pmatrix} p_1^1 & p_1^2 & \cdots & \cdots & p_1^m & -q_1^1 \int_0^1 \phi_1 \psi_1 d\xi & \cdots & -\sum_{j=1}^{m} q_j^m \int_0^1 \phi_j \psi_1 d\xi \\ 0 & p_2^2 & \cdots & \cdots & p_2^m & \cdots & \cdots & \cdots \\ \cdots & \cdots & \cdots & \cdots & \cdots & \cdots & \cdots & \cdots \\ \cdots & \cdots & \cdots & \cdots & \cdots & \cdots & \cdots & \cdots \\ 0 & 0 & \cdots & \cdots & p_m^m & -q_1^1 \int_0^1 \phi_1 \psi_m d\xi & \cdots & -\sum_{j=1}^{m} q_j^m \int_0^1 \phi_j \psi_m d\xi \\ \beta_1^2 p_1^1 \int_0^1 \psi_1 \phi_1 d\xi & \cdots & \beta_m^2 \sum_{j=1}^{m} p_j^m \int_0^1 \psi_j \phi_1 d\xi & \alpha_1^2 q_1^1 & \cdots & \cdots & \alpha_m^2 q_1^m \\ \cdots & \cdots & \cdots & 0 & \alpha_2^2 q_2^2 & \cdots & \alpha_m^2 q_2^m \\ \cdots & \cdots & \cdots & \cdots & \cdots & \cdots & \cdots \\ \cdots & \cdots & \cdots & \cdots & \cdots & \cdots & \cdots \\ \beta_1^2 p_1^1 \int_0^1 \psi_1 \phi_m d\xi & \cdots & \beta_m^2 \sum_{j=1}^{m} p_j^m \int_0^1 \psi_j \phi_m d\xi & 0 & 0 & \cdots & \alpha_m^2 q_m^m \end{pmatrix} \quad (29c)$$

Equation (20) into Equation (11) and carrying out the integration. This yields

$$\bar{\theta}_2 = 4\eta + \frac{8}{N_{Pe}^2} + 4\sum_{n=1}^{\infty} C_n \exp\{-\beta_n^2\eta\} \int_0^1 \xi(1-\xi^2) R_n d\xi$$

$$= 4\eta + \frac{8}{N_{Pe}^2} - \frac{4}{N_{Pe}^2} \sum_{n=1}^{\infty} C_n \beta_n^2 \exp\{-\beta_n^2\eta\} \int_0^1 \xi R_n d\xi \quad (31)$$

the latter simplifying step being obtained by making use of Equation (18). In an analogous manner, the average fluid temperature in the adiabatic region can be found by combining Equations (15*a*), (11), and (16), that is

$$\bar{\theta}_1 = \frac{4}{N_{Pe}^2} \sum_{n=1}^{\infty} B_n \alpha_n^2 \exp\{\alpha_n^2\eta\} \int_0^1 \xi Y_n d\xi \quad (32)$$

It can be seen from Equation (31) that as $\eta \longrightarrow \infty$, $\bar{\theta}_2$ tends to vary linearly with respect to η, as it should. In the thermal entry region, however, the variation is not exactly linear. The numerical values for the integral appearing in Equation (31) have been evaluated and are shown also in Table 1 for $N_{Pe} = 1$ and 5. Of particular interest is the expression for the local Nusselt number in the heated region. It can be derived by noting that the wall temperature in this region is given by

$$[\theta_2]_w = 4\eta + \frac{11}{24} + \frac{8}{N_{Pe}^2} + \sum_{n=1}^{\infty} C_n R_n(1) \exp\{-\beta_n^2\eta\} \quad (33)$$

Combination of Equation (31) and Equation (33) thus leads to

$$N_{Nu_1} = \frac{2r_o}{k} \frac{q_w}{[T_2]_w - T_{av}} = \frac{2}{[\theta_2]_w - \bar{\theta}_2}$$

$$= \frac{2}{\frac{11}{24} + \sum_{n=1}^{\infty} C_n R_n(1) \exp\{-\beta_n^2\eta\} + \frac{4}{N_{Pe}^2} \sum_{n=1}^{\infty} C_n \beta_n^2 \exp\{-\beta_n^2\eta\} \int_0^1 \xi R_n d\xi} \quad (34)$$

Parallel-Plate Channel Flow

For the corresponding problem in parallel-plate channel flow, the governing energy equations, in dimensionless form, can be written as

$$(1-\xi^2)\frac{\partial\theta_i}{\partial\eta} = \frac{\partial^2\theta_i}{\partial\xi^2} + \left(\frac{8}{3N_{Pe}}\right)^2 \frac{\partial^2\theta_i}{\partial\eta^2} \quad (i = 1, 2) \quad (35)$$

where $\theta_i = (T - T_o)/(q_w a/k)$ $(i = 1, 2)$, $\xi = y/a$, $\eta = 8x/3aN_{Pe}$, $N_{Pe} = 4a\bar{u}\rho C_p/k$, and a is one-half the channel height. With the understanding of the differences in notations, the boundary conditions given by Equations (6) to (8) in the previous section are directly applicable here. The fully developed temperature solution θ_{fd} in this case, however, takes the form

$$\theta_{fd} = \frac{3}{2}\eta + \frac{3}{4}\xi^2 - \frac{\xi^4}{8} - \frac{39}{280} + \frac{16}{N_{Pe}^2} \quad (36)$$

which can be derived, as before, by taking a heat balance. Denoting the temperature solutions in the adiabatic and heated regions by

For $-\infty < \eta \leq 0$:

$$\theta_1 = \sum_{n=1}^{\infty} B_n Y_n(\xi) \exp[\alpha_n^2\eta] \quad (37a)$$

For $0 \leq \eta < \infty$:

$$\theta_2 = \frac{3}{2}\eta + \frac{3}{4}\xi^2 - \frac{\xi^4}{8} - \frac{39}{280} + \frac{16}{N_{Pe}^2} + \sum_{n=1}^{\infty} C_n R_n(\xi) \exp[-\beta_n^2\eta] \quad (37b)$$

the characteristic equations for the eigenvalues and eigenfunctions are now given by

$$\frac{d^2Y_n}{d\xi^2} + \alpha_n^2[(8\alpha_n/3N_{Pe})^2 - (1-\xi^2)]Y_n = 0 \quad (38a)$$

$$\frac{dY_n}{d\xi} = 0 \quad \text{at } \xi = 0 \text{ and } \xi = 1 \quad (38b)$$

and

$$\frac{d^2R_n}{d\xi^2} + \beta_n^2[(8\beta_n/3N_{Pe})^2 + (1-\xi^2)]R_n = 0 \quad (39a)$$

$$\frac{dR_n}{d\xi} = 0 \quad \text{at } \xi = 0 \text{ and } \xi = 1 \quad (39b)$$

The computed first 20 eigenvalues α_n and β_n for $N_{Pe} = 1$ and 5 are tabulated in Table 4.*

Once again, two new orthonormal sets of functions ψ_n and ϕ_n are constructed from the nonorthogonal eigenfunctions R_n and Y_n. Some of the computed numerical constants a_n^j, b_n^j, p_n^j, q_n^j for $N_{Pe} = 1$ and 5 are tabulated in Tables 5* and 6* for reference. The method of determining the series expansion coefficients C_n's and B_n's is exactly identical to that described in the previous section and will not be repeated here. The sets of simultaneous equations which give rise to the final matrix equations, in this case, take the form

$$\sum_{j=m}^{\infty} C_j p_m^j - \sum_{n=1}^{\infty} \sum_{j=n}^{\infty} B_j q_n^j \int_0^1 \phi_n \psi_m d\xi = -\int_0^1 \left(\frac{3}{4}\xi^2 - \frac{\xi^4}{8} - \frac{39}{280} + \frac{16}{N_{Pe}^2}\right)\psi_m d\xi \quad (40a)$$

$$\sum_{j=m}^{\infty} B_j \alpha_j^2 q_m^j + \sum_{n=1}^{\infty} \sum_{j=n}^{\infty} C_j \beta_j^2 p_n^j \int_0^1 \psi_n \phi_m d\xi = 1.5 \int_0^1 \phi_m d\xi \quad (m = 1, 2, \ldots) \quad (40b)$$

Upon terminating the infinite series appearing in Equations (40*a*) and (40*b*) at $m = 20$, the B_n and C_n coefficients were determined and the results for $N_{Pe} = 1$ and 5 are tabulated in Table 4. By going through the similar derivation

*See footnote on p. 734.

as before for the local Nusselt number, one now obtains

$$N_{Nu_2} = \frac{4a}{k}\frac{q_w}{[T_2]_w - T_{av}} = \frac{4}{[\theta_2]_w - \bar{\theta}}$$

$$= \frac{4}{\frac{17}{35} + \sum_{n=1}^{\infty} C_n R_n(1) \exp\{-\beta_n^2 \eta\} + \frac{32}{3N_{Pe}^2} \sum_{n=1}^{\infty} C_n \beta_n^2 \exp\{-\beta_n^2 \eta\} \int_0^1 R_n d\xi} \tag{41}$$

Some of the numerical values of the integral appearing in Equation (41) are shown in Table 4 for $N_{Pe} = 1$ and 5.

DISCUSSIONS OF RESULTS AND CONCLUSIONS

To illustrate how the series expansion coefficients C_n and B_n satisfy the matching conditions required at $x = 0$, these coefficients were used to calculate the left-hand side of both Equations (21*a*) and (21*b*). The calculated results are plotted in Figure 5 for the case of $N_{Pe} = 1$ and compared with the right-hand side of the two equations. As can be observed, the two matching conditions are both fulfilled very well. This is, in fact, a direct proof of the mathematical correctness of the present solution. Upon substituting these coefficients and the computed eigenconstants into Equation (34), the theoretical Nusselt numbers in the thermal entry region can be calculated. The Nusselt curves thus constructed are shown in Figure 6 for $N_{Pe} = 1$, 2.5, 5, 10, 20, 30, 45, and ∞ (no axial conduction). Originally, it was intended to plot also the Nusselt curves obtained by Hennecke (*3*) for $N_{Pe} = 1$, 5, 10, and 20. However, the agreement between his results and the theoretical Nusselt numbers obtained in this study is so good that it is essentially impossible to show graphically any difference between them. As remarked previously, Hennecke's results were obtained by solving the partial differential equation directly using the finite-difference methods. In Figure 7 the Nusselt curves obtained by Petukhov and Tsvetkov (*7*) for N_{Pe} of 1, 10, and 45 are sketched and compared with those obtained in this study. The former curves were also obtained by solving the governing differential equation by a numerical method. For low values of the axial distance pa-

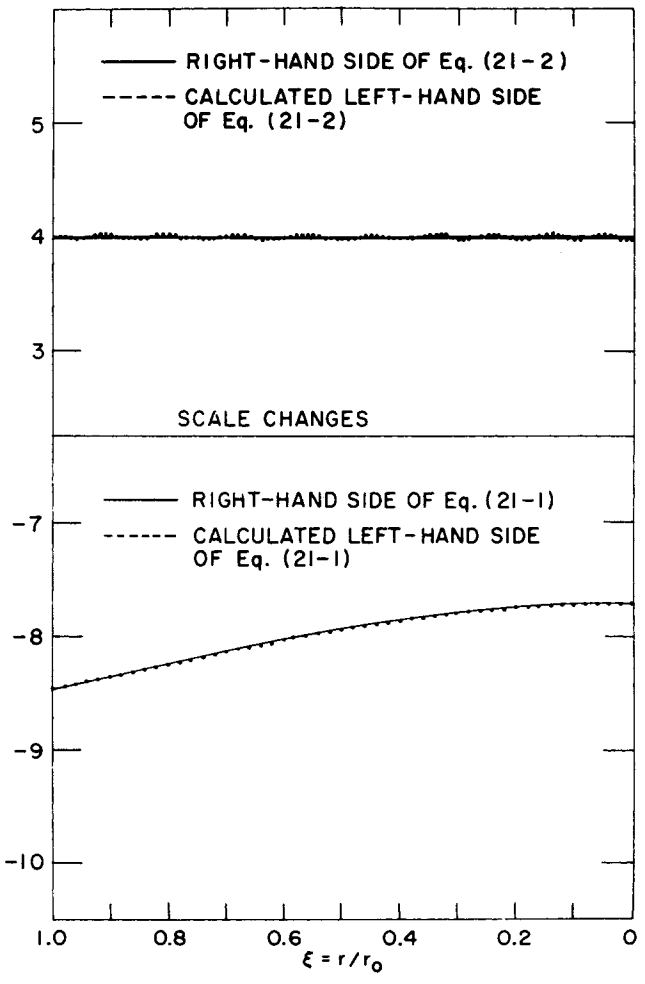

Fig. 5. Results of matching the temperatures and temperature gradients at x = 0 for pipe flow ($N_{Pe} = 1$).

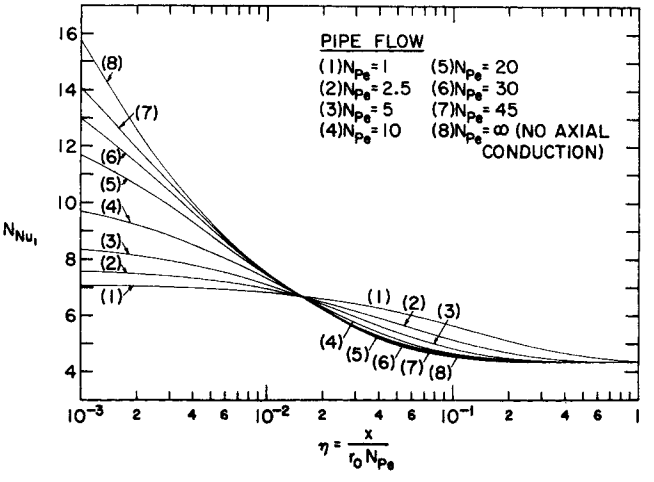

Fig. 6. Thermal entry region local Nusselt number for pipe flow.

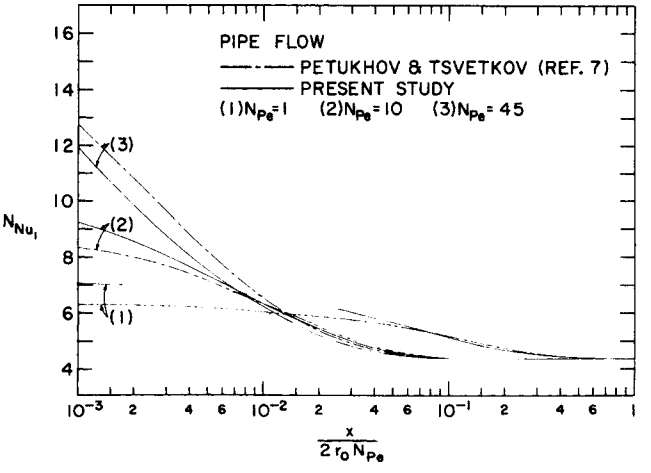

Fig. 7. Comparison of Nusselt curves.

rameter $x/2r_oN_{Pe}$, it can be seen that the curve obtained by Petukhov and Tsvetkov for $N_{Pe} = 45$ is ≈8% higher, while the curves for $N_{Pe} = 1$ and 10 are roughly 10% lower than those obtained in this study.

It is of particular interest to observe the dependence of the thermal entry region Nusselt numbers upon the boundary condition imposed at $x = 0$. If the fluid temperature is assumed to be uniform at $x = 0$, as was done in the previous study (*4*), then, from the definition of the heat transfer coefficient, it is apparent that the Nusselt number should approach infinity as $\eta \longrightarrow 0$, regardless of Peclet number. The Nusselt curves corresponding to different values of the Peclet number thus do not cross each other at small values of η. However, if upstream conduction into the adiabatic region is taken into account, the radial distribution of fluid temperature at $x = 0$ tends to deviate more and more from uniformity, as Peclet number becomes smaller. Such nonuniformity eventually causes the difference between wall temperature and bulk fluid temperature at $x = 0$ to increase, as the Peclet number is lowered. This is the main reason why the Nusselt curves shown in Figure 6 cross each other and reverse their order of relative magnitude at small values of η. The assumption of a flat temperature profile at $x = 0$ can thus be seen to cause considerable errors in the prediction of local Nusselt numbers near $\eta = 0$. It is of some interest to note from Figure 6 that for pipe flow, all the crossing takes place near a single point, at $\eta \cong 0.015$.

In Figures 8 and 9 longitudinal variation of fluid temperature is shown for the case of $N_{Pe} = 1$ and 45. These curves were obtained by using Equations (15*a*) and (20). In the adiabatic region the temperature profiles for both cases are seen to be flat at sufficiently large $|\eta|$. For the case of $N_{Pe} = 45$, in which the effect of upstream conduction is relatively small, such uniformity is roughly maintained until

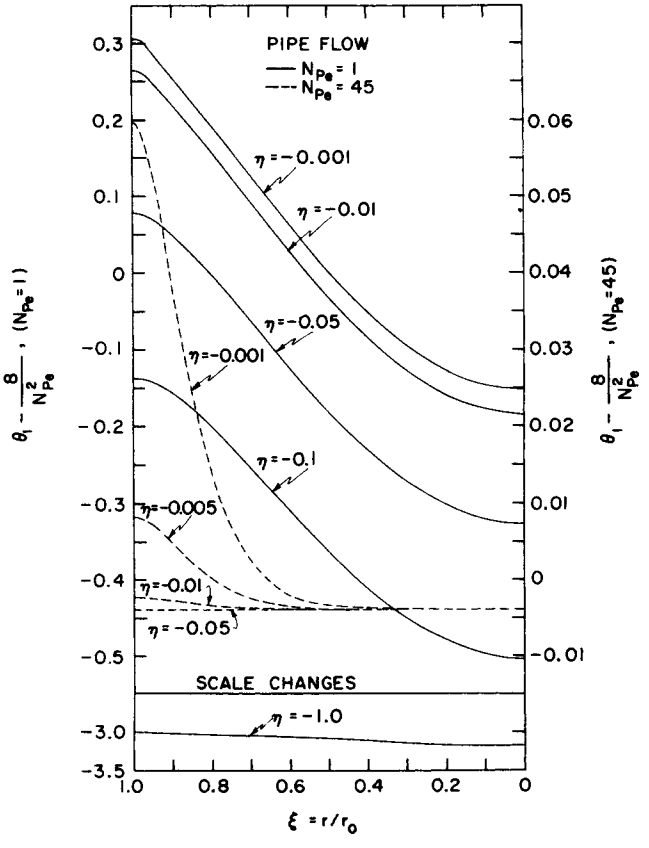

Fig. 8. Distribution of fluid temperature in the adiabatic region for pipe flow (N_{Pe} = 1 and 45).

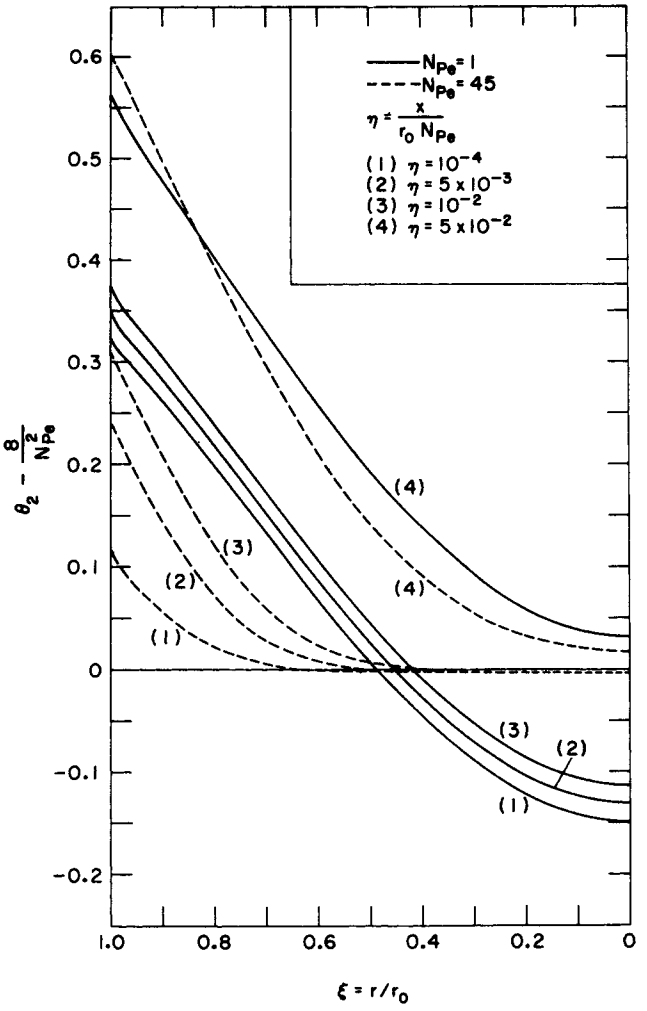

Fig. 9. Distribution of fluid temperature in the heated region for pipe flow (N_{Pe} = 1 and 45).

η becomes larger than −0.01, where the effect of axial conduction starts to become evident. In the region $-0.01 \leq \eta \leq 0$, it can be observed that the heat conducted upstream causes a rather sharp increase in wall temperature, while the fluid temperature near the center of the channel remains very little affected. This is presumably because the effect of axial conduction is more significant near the wall due to the heat source located at the wall in the region $x \geq 0$, and that fluid velocity is relatively low in the region near the wall. Furthermore, for the region near the center of the channel, the heat conducted upstream is rapidly transported back downstream. As a whole, the average fluid temperature of the flowing stream rises only slightly. That this is not the case for $N_{Pe} = 1$ can be clearly seen from the figures. For such a small Peclet number, the amount of heat conducted upstream is so large that the average fluid temperature in the adiabatic region continues to rise along the longitudinal distance. It is interesting to note that the fluid temperature is now affected in the entire region extending from the center of the channel to the pipe wall. It is also noted that in the region, $-0.1 < \eta < 0.05$, the temperature profile retains approximately the same shape. In this region therefore the net heat input into a fluid element due to the combined conduction and convection remains approximately constant along the axial distance. This is primarily the reason why the Nusselt number for $N_{Pe} = 1$ varies very little in the region close to $\eta = 0$. For $N_{Pe} = 45$, on the other hand, the wall temperature continues to rise in

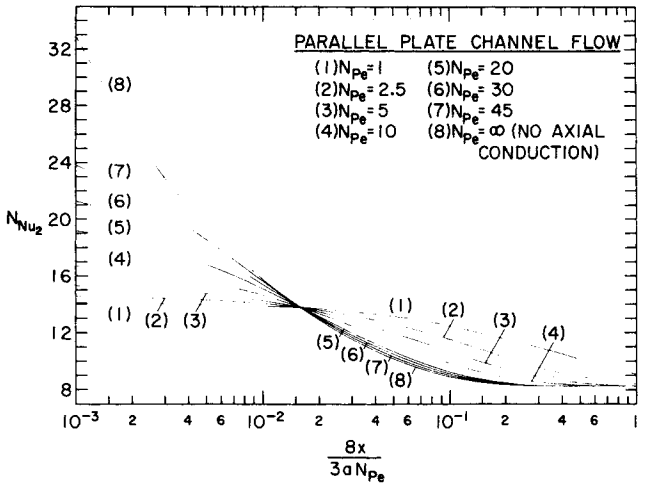

Fig. 10. Thermal entry region local Nusselt number for parallel-plate channel flow.

the heated region, thus causing the Nusselt number to decrease more rapidly.

In Figure 10, the Nusselt curves obtained from Equation (41) are shown for the case of parallel-plate channel flow. It can be observed that the heat transfer behavior is very similar to that for the pipe flow. The crossing of the Nusselt number curves, in this case occurs at $8x/3aN_{Pe} \cong 0.016$.

ACKNOWLEDGMENT

This work was performed under the auspices of the U.S. Atomic Energy Commission.

NOTATION

B_n = coefficients of series expansion in Equation (15*a*) for pipe flow, or in Equation (37*a*) for parallel-plate channel flow

C_n = coefficients of series expansion in Equation (15*b*) for pipe flow, or in Equation (37*b*) for parallel-plate channel flow

C_p = specific heat

$\vec{E}$ = matrix as defined by Equation (29*c*)

$\vec{F}$ = matrix as defined by Equation (29*a*)

$\vec{G}$ = matrix as defined by Equation (29*b*)

$N_{Nu_1} = \frac{2r_o}{k}\frac{q_w}{[T_2]_w - T_{av}}$, local Nusselt number for pipe flow

$N_{Nu_2} = \frac{4a}{k}\frac{q_w}{[T_2]_w - T_{av}}$, local Nusselt number for parallel-plate channel flow

N_{Pe} = Peclet number, $= (2r_o\rho C_p\bar{u})/k$ for pipe flow, $= (4a\bar{u}\rho C_p)/k$ for parallel-plate channel flow

R_n = eigenfunctions for Equations (18) and (19), or for Equations (39*a*) and (39*b*)

T_{av} = bulk fluid temperature in the heated region

$T_i (i = 1, 2)$ = fluid temperature in the adiabatic and heated region, respectively

T_o = uniform inlet fluid temperature

T_{fd} = fully developed fluid temperature in the heated region

$[T_2]_w$ = wall temperature in the heated region

Y_n = eigenfunctions for Equations (16) and (17) or for Equations (38*a*) and (38*b*)

a = one-half the parallel-plate channel height

a_n^j = coefficients in Equation (22*a*)

b_n^j = coefficients in Equation (22*b*)

$f_1(\xi) = -\left(\xi^2 - \frac{\xi^4}{4} - \frac{7}{24} + \frac{8}{N_{Pe}^2}\right)$

k = thermal conductivity

p_n^j = coefficients in Equation (26*a*)

q_n^j = coefficients in Equation (26*b*)

q_w = wall heat flux

r = radial distance

r_o = radius of a pipe

$\bar{u}$ = average fluid velocity

x = axial position

Greek Letters

α_n = eigenvalues of Equations (16) and (17), or of Equations (38*a*) and (38*b*)

β_n = eigenvalues of Equations (18) and (19), or of Equations (39*a*) and (39*b*)

Δ_n = determinant as defined by Equation (25)

$\eta = x/r_oN_{Pe}$ for pipe flow, and $= 8x/3aN_{Pe}$ for parallel-plate channel flow

$\theta_i (i = 1, 2) = (T_i - T_o)/(q_w r_o/k)$, dimensionless temperatures

θ_η = dimensionless fluid temperature at a location η

$\bar{\theta}_\eta$ = dimensionless average fluid temperature at a location η

θ_{fd} = dimensionless fluid temperature in the fully developed region

$\bar{\theta}_{fd}$ = dimensionless average fluid temperature in the fully developed region

$\bar{\theta}_1$ = dimensionless average fluid temperature in the adiabatic region

$\bar{\theta}_2$ = dimensionless average fluid temperature in the heated region

$\Theta_2 = \theta_2 - \theta_{fd}$

$[\theta_2]_w$ = dimensionless wall temperature in the heated region

$\xi = r/r_o$ for pipe flow, and $= y/a$ for parallel-plate channel flow

ρ = density of fluid

ϕ_n = orthonormal system as defined by Equation (22*b*)

ψ_n = orthonormal system as defined by Equation (22*a*)

LITERATURE CITED

1. Agrawal, H. C., *Appl. Sci. Res.*, **A9**, 177 (1960).
2. Bird, R. B., W. E. Stewart, and E. N. Lightfoot, "Transport Phenomena," p. 296, Wiley, New York (1960).
3. Hennecke, D. K., *Wärme-Stoffübertragung Bd.*, **1**, 177 (1968).
4. Hsu, C.-J., *Appl. Sci. Res.*, **17**, 359 (1967).
5. McMordie, R. K., and A. F. Emery, *Trans. ASME J. Heat Transfer*, **89c**, 11 (1967).
6. Natanson, I. P., "Theory of Functions of a Real Variable" (Transl. by Boron, L. F.), Vol. 1, p. 195, rev. edit., Frederick Ungar, New York (1961).
7. Petukhov, B. S., and F. F. Tsvetkov, *Inz.-Fiz. Zh.*, **4**, 10–17 (1961); *Transl. No. FTD TT-61-321* (Jan. 29, 1962).
8. Schneider, P. J., *Trans. ASME*, **79**, 766 (1957).
9. Singh, S. N., *Appl. Sci. Res.*, **A7**, 237 (1957).
10. *Ibid.*, p. 325.

Manuscript received July 17, 1969; revision received September 4, 1969; paper accepted September 10, 1969.